

# Quality-Guided Semi-Supervised Learning for Medical Image Segmentation

Kumar Abhishek<sup>[0000-0002-7341-9617]</sup> and Ghassan Hamarneh<sup>[0000-0001-5040-7448]</sup>

School of Computing Science, Simon Fraser University, Canada  
{kabhishe,hamarneh}@sfu.ca

**Abstract.** Training accurate medical image segmentation models requires large amounts of densely annotated data, which is costly and time-consuming to obtain. Semi-supervised learning (SSL) alleviates this by learning from both abundant unlabeled data and limited labeled data. However, most modern SSL methods rely on pseudolabels for unlabeled data, and typically assess their reliability through model confidence or uncertainty, measures that are self-referential and lack explicit grounding in segmentation quality. Instead, we propose a *quality*-guided SSL framework that trains a dedicated network to estimate segmentation quality from image-mask pairs. The predictor is trained on variable-quality masks generated through synthetic corruptions augmented with imperfect outputs from partially trained segmentation models, capturing realistic error patterns encountered during training. We integrate the quality predictor into SSL through two complementary mechanisms: a quality-aware regularization loss and a quality-based pseudolabel sample reweighting scheme. We show that our method serves as a drop-in enhancement to existing SSL frameworks. Extensive experiments across five datasets and multiple architectures demonstrate consistent improvements over competing SSL methods, advancing the state-of-the-art in semi-supervised medical image segmentation.

**Keywords:** Image segmentation · Segmentation quality · Semi-supervised learning.

## 1 Introduction

Accurate segmentation of medical images is fundamental to clinical workflows, yet dense pixelwise annotations, necessary for training deep learning-based segmentation models, remain costly and scarce [22,38,1]. Semi-supervised learning (SSL) addresses this annotation scarcity by leveraging abundant unlabeled data alongside limited labels, and has become a dominant paradigm for label-efficient medical image segmentation.

Most existing SSL approaches differ in how they leverage unlabeled data, falling into three broad categories: (i) consistency regularization, enforcing prediction invariance under perturbations, notably mean teacher (MT) [39], its

uncertainty-aware extension (UA-MT) [42], and interpolation consistency training (ICT) [41]; (ii) pseudolabel methods, using confident predictions as surrogate supervision [19,35], extended by cross-pseudo supervision (CPS) [9]; and (iii) contrastive learning, leveraging representation-level objectives on unlabeled data [7]. Across these methods, unlabeled samples are either treated uniformly regardless of prediction quality (MT, ICT), or filtered using model-derived confidence as a proxy for reliability (UA-MT, FixMatch [35]). Although calibration techniques can reduce overconfidence [15], medical segmentation networks remain poorly calibrated in practice [24]. More fundamentally, even perfectly calibrated confidence is self-referential, since it reflects the model’s belief about its own prediction, and cannot catch systematic errors arising from the same representations that produced them. We argue that an independent assessment of segmentation quality is a better alternative to model certainty for guiding SSL training.

Predicting segmentation quality without ground truth has been studied for clinical quality control. Early work predicted Dice scores from hand-crafted features [18] and reverse classifiers to estimate quality [40]. More recent approaches directly regress quality metrics from image-segmentation pairs [30,10,28], and large-scale models now offer general-purpose quality prediction across diverse anatomies [33]. However, this entire line of work treats quality prediction as an end goal, filtering unreliable segmentations post-hoc. No prior work has leveraged learned quality prediction to guide semi-supervised training itself.

We bridge these two directions by training a quality predictor that estimates segmentation quality from image-mask pairs, then using it to provide learning signal for unlabeled data in SSL. Unlike confidence from a single forward pass, predicted quality provides a complementary signal by comparing mask structure against image evidence, independently of the segmentation network’s own representations. While related to sample reweighting for noisy labels [29,34], our predictor directly estimates segmentation accuracy rather than inferring importance from per-sample loss values. However, a quality predictor trained on variable quality masks from labeled data must generalize to real network predictions of unlabeled data.

To provide a quality-based guidance for medical image segmentation in a semi-supervised setting, we contribute: (1) the first framework-agnostic method to leverage learned segmentation quality prediction for guiding SSL; (2) two complementary mechanisms for integrating quality predictions into SSL training: a differentiable quality regularizer and a pseudolabel reweighting scheme, applicable as drop-in enhancements to existing SSL methods; (3) a mask corruption strategy incorporating partially-trained model predictions that exhibit characteristic neural network errors [5,17] to bridge the distribution gap between synthetic and real network errors; and (4) we perform comprehensive experiments across five cross-dataset pairs spanning dermatology and colonoscopy, five SSL paradigms, and multiple model architectures, yielding consistent improvements over state-of-the-art baselines. Our code is publicly available at <https://github.com/sfu-mial/QG-SSL>.

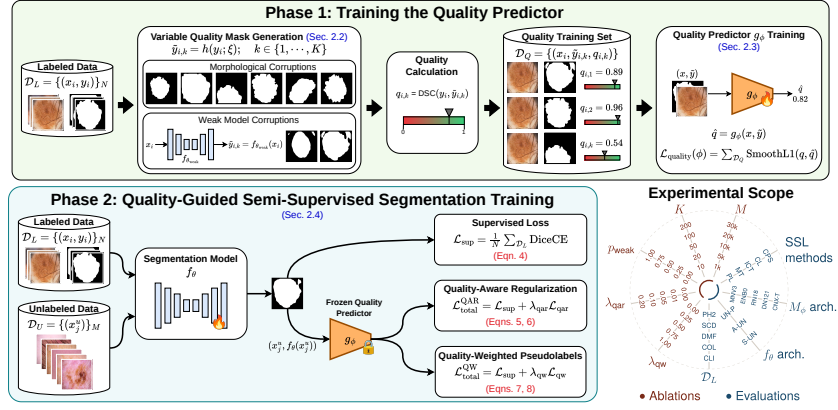


**Fig. 1.** An overview of the proposed quality-guided semi-supervised segmentation methods, along with the scope of experiments present in this paper.

## 2 Method

Our proposed approach has two phases: (Phase 1) training a quality predictor  $g_\phi$  to estimate segmentation quality from image-mask pairs, and (Phase 2) using the frozen  $g_\phi$  to guide semi-supervised segmentation training. Fig. 1 provides an overview and the scope of experiments presented in this paper.

### 2.1 Problem Definition

Let  $\mathcal{D}_L = \{(x_i, y_i)\}_{i=1}^N$  denote a small labeled set, where  $x_i \in \mathbb{R}^{H \times W \times C}$  is an image and  $y_i \in \{0, 1\}^{H \times W}$  is its ground truth binary segmentation mask, and let  $\mathcal{D}_U = \{x_j^u\}_{j=1}^M$  ( $M \gg N$ ) be a larger unlabeled set. Our goal is to train a segmentation network  $f_\theta$  that leverages both  $\mathcal{D}_L$  and  $\mathcal{D}_U$ . In our experiments,  $\mathcal{D}_L$  and  $\mathcal{D}_U$  come from related but distinct sources (e.g., PH2 [25] and ISIC2020 [32]), a challenging setting that better reflects clinical practice. We do not assume matched distributions between labeled and unlabeled data.

### 2.2 Variable Quality Mask Generation

To train  $g_\phi$ , we require images paired with arbitrary masks, where each mask has a corresponding quality score. We construct a synthetic dataset  $\mathcal{D}_Q$  from  $\mathcal{D}_L$  by generating, for each  $(x_i, y_i) \in \mathcal{D}_L$ , a set of  $K$  degraded masks using a stochastic corruption function  $h$ :

$$\tilde{y}_{i,k} = h(y_i; \xi_k), \quad q_{i,k} = \text{DSC}(y_i, \tilde{y}_{i,k}), \quad k \in \{1, \dots, K\}, \quad (1)$$

where  $\xi_k$  represents random perturbation parameters, and  $q_{i,k} \in [0, 1]$  is the Dice score (DSC) of each corrupted mask. We sample two types of degradations randomly. First (Type 1), we use random morphological operations (erosion/dilation with different kernel sizes), translations, elastic deformations, additive noise, and boundary perturbations. However, morphological corruptions

alone may not capture error patterns produced by real neural networks during semi-supervised training. To bridge this distribution gap, (Type 2) we augment our corruption strategy with predictions from partially trained (weak) segmentation models  $f_{\theta_{\text{weak}}}$ . We train a U-Net [31] on  $\mathcal{D}_L$  from random initialization and collect checkpoints at early epochs (epochs 1, 3, 5, 10, 15, 20). These weak models produce segmentation predictions exhibiting characteristic early training failure patterns [17,5]. Previous work on learned quality prediction has also noted that limited corruption diversity restricts the predictor’s sensitivity to fine-grained quality differences [30], further motivating the inclusion of real network outputs of imperfect segmentation models. Therefore, when training  $g_\phi$ , we sample with probability  $p_{\text{weak}}$  from these weak-model predictions (Type 2) and  $1 - p_{\text{weak}}$  from Type 1 corruptions. The resulting dataset  $\mathcal{D}_Q = \{(x_i, \tilde{y}_{i,k}, q_{i,k})\}$  contains image-mask-quality triplets spanning the full range of Dice scores. We explore various settings of  $p_{\text{weak}}$  and  $K$ .

### 2.3 Segmentation Quality Predictor

The quality predictor  $g_\phi$  takes an image-mask pair, outputs a scalar quality estimate (Eqn. 2) and is trained to minimize a regression loss  $\ell_{\text{reg}}$  (Eqn. 3):

$$\hat{q} = g_\phi(x, \tilde{y}), \quad (2)$$

$$\mathcal{L}_{\text{quality}}(\phi) = \sum_{(x, \tilde{y}, q) \in \mathcal{D}_Q} \ell_{\text{reg}}(g_\phi(x, \tilde{y}), q). \quad (3)$$

A key property distinguishing quality prediction from proxy signals such as model confidence is that it is designed to be contextually grounded: to assess whether  $\tilde{y}$  is a good segmentation of  $x$ ,  $g_\phi$  must compare mask structure against visual evidence in the image, rather than relying on the mask or the model’s internal state alone. Once trained,  $g_\phi$  is frozen and acts as a differentiable quality assessment function for any image-mask pair without requiring ground truth.

### 2.4 Quality-Guided Semi-Supervised Training

We now train  $f_\theta$  using both  $\mathcal{D}_L$  and  $\mathcal{D}_U$ . For all labeled samples, we minimize:

$$\mathcal{L}_{\text{sup}}(\theta) = \frac{1}{N} \sum_{i=1}^N \ell_{\text{seg}}(f_\theta(x_i), y_i). \quad (4)$$

For unlabeled data, we propose two alternative mechanisms for leveraging the frozen  $g_\phi$ , differing in whether the segmentation loss  $\ell_{\text{seg}}$  gradients propagate through  $g_\phi$  (QAR) or  $g_\phi$  serves only to compute per-sample weights (PL-QW).

**A: Quality-Aware Regularization (QAR):** For each unlabeled sample  $x_j^u$ , the soft prediction  $f_\theta(x_j^u)$  is passed into  $g_\phi$ . No explicit pseudolabels are generated; instead, gradients of the loss  $\mathcal{L}_{\text{qar}}$  propagate from the scalar quality output

back through the predicted mask into segmentation model parameters  $\theta$ , encouraging  $f_\theta$  to produce segmentations that  $g_\phi$  judges as high quality:

$$\mathcal{L}_{\text{qar}}(\theta) = \frac{1}{M} \sum_{j=1}^M (1 - g_\phi(x_j^u, f_\theta(x_j^u))). \quad (5)$$

The complete objective is a weighted sum of the two losses:

$$\mathcal{L}_{\text{total}}^{\text{QAR}} = \mathcal{L}_{\text{sup}} + \lambda_{\text{qar}} \mathcal{L}_{\text{qar}}. \quad (6)$$

**B: Quality-Weighted Pseudolabels (PL-QW):** Given pseudolabels  $\hat{y}_j^u$  for unlabeled samples  $x_j^u \in \mathcal{D}_U$ , we weight the per-sample loss by predicted pseudolabel quality:

$$\mathcal{L}_{\text{qw}}(\theta) = \frac{1}{M} \sum_{j=1}^M w_j \cdot \ell_{\text{seg}}(f_\theta(x_j^u), \hat{y}_j^u), \quad (7)$$

where  $w_j = g_\phi(x_j^u, \hat{y}_j^u)$  is computed with  $g_\phi$  frozen and detached from the computational graph. Unlike QAR, no gradients flow through  $g_\phi$ ; it serves purely as a sample weighting function that upweights high-quality pseudolabels and downweights unreliable ones. The complete objective is:

$$\mathcal{L}_{\text{total}}^{\text{QW}} = \mathcal{L}_{\text{sup}} + \lambda_{\text{qw}} \mathcal{L}_{\text{qw}}. \quad (8)$$

A key property of this formulation is its orthogonality to the choice of semi-supervised method: any approach generating pseudolabels  $\hat{y}_j^u$  can be augmented by weighting per-sample losses with  $w_j$ , without requiring architectural changes.

### 3 Results and Discussion

**Datasets:** We study 5 medical image segmentation datasets from two modalities as labeled data  $\mathcal{D}_L$ : PH2 ( $N=200$ ) [25], Skin Cancer Detection (SCD;  $N=206$ ) [14], and DermoFit (DMF;  $N=1,300$ ) [2] for skin lesion segmentation, and CVC-ColonDB (COL;  $N=380$ ) [4] and CVC-ClinicDB (CLI;  $N=612$ ) [3] for polyp segmentation in colonoscopy. All datasets are split 70:10:20 for train, validation, and test. As unlabeled data  $\mathcal{D}_U$ , we use ISIC2020-Train ( $M=33,126$ ) [32] and Polyp-Box-Seg ( $M=4,070$ ) [8] for dermatology and colonoscopy respectively: both drawn from different sources than  $\mathcal{D}_L$ . We use 5,000 ISIC2020 images for main experiments (Table 1) and the remainder for hyperparameter sensitivity analyses (Table 2). All models were trained on Ubuntu 22.04 with Intel Core i9-14900K, 64GB RAM, NVIDIA RTX4090, Python 3.10.19, and PyTorch 2.9.0. **Quality predictor training and evaluation:** We implement  $g_\phi$  as a ResNet-18 encoder, that takes the channel-wise concatenation of image-mask pairs as input, with a regression head (dropout of 0.15), trained for 150 epochs with AdamW [23] (learning rate=3e-4, weight decay=5e-4, batch size 32) with cosine

**Table 1.** Quantitative results (DSC and IoU; mean<sub>std.err.</sub>) for all SSL baselines, their quality-weighted versions, and QAR. Using a quality predictor consistently improves segmentation performance across 5 datasets and 3 segmentation model architectures.

| $\mathcal{D}_L$ | $f_\theta$<br>Arch. | Pseudolabels |                       |                       | Student-Teacher Models |                       |                       | Interp. Consistency   |                       | Contrastive           |                       | Cross Pseudo Sup.     |                       | QAR<br>(Ours)         |                       |                       |                       |
|-----------------|---------------------|--------------|-----------------------|-----------------------|------------------------|-----------------------|-----------------------|-----------------------|-----------------------|-----------------------|-----------------------|-----------------------|-----------------------|-----------------------|-----------------------|-----------------------|-----------------------|
|                 |                     | SUP          | PL-T<br>[19]          | PL-C<br>[35]          | PL-QW<br>(Ours)        | MT<br>[39]            | UA-MT<br>[42]         | MT-QW<br>(Ours)       | ICT<br>[41]           | ICT-QW<br>(Ours)      | CL<br>[7]             | CL-QW<br>(Ours)       | CPS<br>[9]            |                       | CPS-QW<br>(Ours)      |                       |                       |
| PH2             | UN-P                | DSC          | 92.93 <sub>0.52</sub> | 93.21 <sub>0.88</sub> | 93.92 <sub>1.10</sub>  | 95.46 <sub>0.23</sub> | 93.53 <sub>1.62</sub> | 94.33 <sub>0.62</sub> | 95.32 <sub>0.23</sub> | 93.85 <sub>0.82</sub> | 95.18 <sub>0.16</sub> | 92.37 <sub>1.82</sub> | 94.48 <sub>0.36</sub> | 94.20 <sub>0.71</sub> | 95.19 <sub>0.52</sub> | 95.48 <sub>0.28</sub> |                       |
|                 |                     | IoU          | 86.96 <sub>0.83</sub> | 87.75 <sub>1.41</sub> | 89.19 <sub>1.58</sub>  | 91.45 <sub>0.79</sub> | 89.04 <sub>0.00</sub> | 89.51 <sub>1.04</sub> | 91.18 <sub>0.78</sub> | 88.81 <sub>1.30</sub> | 90.95 <sub>0.81</sub> | 87.23 <sub>2.12</sub> | 89.75 <sub>0.97</sub> | 89.46 <sub>1.16</sub> | 91.01 <sub>0.91</sub> | 91.50 <sub>0.84</sub> |                       |
|                 | A-UN                | DSC          | 91.73 <sub>0.69</sub> | 92.90 <sub>0.67</sub> | 93.34 <sub>0.82</sub>  | 95.40 <sub>0.23</sub> | 93.18 <sub>1.60</sub> | 93.70 <sub>0.64</sub> | 95.38 <sub>0.24</sub> | 94.16 <sub>0.38</sub> | 95.17 <sub>0.29</sub> | 92.91 <sub>1.88</sub> | 95.09 <sub>0.48</sub> | 93.91 <sub>0.70</sub> | 94.99 <sub>0.58</sub> | 95.29 <sub>0.27</sub> | 95.29 <sub>0.27</sub> |
|                 |                     | IoU          | 85.01 <sub>1.18</sub> | 87.17 <sub>1.12</sub> | 87.92 <sub>1.29</sub>  | 91.33 <sub>0.40</sub> | 88.40 <sub>1.36</sub> | 88.41 <sub>1.09</sub> | 91.31 <sub>0.78</sub> | 89.18 <sub>0.89</sub> | 90.95 <sub>0.86</sub> | 88.28 <sub>2.00</sub> | 90.80 <sub>0.84</sub> | 88.83 <sub>1.16</sub> | 90.64 <sub>0.89</sub> | 91.15 <sub>0.86</sub> | 91.15 <sub>0.86</sub> |
|                 | S-UN                | DSC          | 93.02 <sub>0.33</sub> | 94.50 <sub>0.75</sub> | 94.86 <sub>0.50</sub>  | 95.57 <sub>0.11</sub> | 94.90 <sub>0.27</sub> | 94.87 <sub>0.16</sub> | 95.36 <sub>0.21</sub> | 94.69 <sub>0.50</sub> | 95.26 <sub>0.19</sub> | 93.63 <sub>0.85</sub> | 95.70 <sub>0.79</sub> | 94.32 <sub>0.19</sub> | 95.45 <sub>0.44</sub> | 95.58 <sub>0.18</sub> | 95.58 <sub>0.18</sub> |
|                 |                     | IoU          | 87.14 <sub>0.94</sub> | 90.05 <sub>1.02</sub> | 90.39 <sub>0.87</sub>  | 91.63 <sub>0.74</sub> | 90.63 <sub>0.84</sub> | 90.30 <sub>0.81</sub> | 91.27 <sub>0.78</sub> | 90.08 <sub>0.89</sub> | 91.05 <sub>0.78</sub> | 89.21 <sub>1.95</sub> | 91.86 <sub>0.78</sub> | 89.42 <sub>0.85</sub> | 91.42 <sub>0.78</sub> | 91.66 <sub>0.78</sub> | 91.66 <sub>0.78</sub> |
| SCD             | UN-P                | DSC          | 89.88 <sub>0.85</sub> | 91.39 <sub>1.84</sub> | 91.87 <sub>1.16</sub>  | 93.18 <sub>0.79</sub> | 91.46 <sub>1.19</sub> | 92.20 <sub>0.69</sub> | 92.91 <sub>0.88</sub> | 91.86 <sub>1.31</sub> | 93.61 <sub>0.80</sub> | 92.37 <sub>1.13</sub> | 92.67 <sub>0.08</sub> | 90.06 <sub>0.80</sub> | 93.26 <sub>0.78</sub> | 93.24 <sub>0.69</sub> |                       |
|                 |                     | IoU          | 82.15 <sub>1.48</sub> | 85.70 <sub>0.81</sub> | 85.73 <sub>0.71</sub>  | 87.57 <sub>1.18</sub> | 85.08 <sub>1.76</sub> | 86.05 <sub>1.45</sub> | 87.22 <sub>1.84</sub> | 85.87 <sub>0.84</sub> | 88.16 <sub>0.87</sub> | 86.52 <sub>1.89</sub> | 86.96 <sub>0.54</sub> | 82.39 <sub>1.40</sub> | 87.72 <sub>1.24</sub> | 87.63 <sub>1.11</sub> |                       |
|                 | A-UN                | DSC          | 90.89 <sub>0.80</sub> | 91.71 <sub>1.08</sub> | 91.83 <sub>1.02</sub>  | 93.15 <sub>0.76</sub> | 92.23 <sub>1.22</sub> | 92.40 <sub>0.90</sub> | 93.06 <sub>0.81</sub> | 92.34 <sub>0.89</sub> | 93.04 <sub>0.79</sub> | 92.42 <sub>0.82</sub> | 92.64 <sub>0.88</sub> | 92.64 <sub>0.78</sub> | 92.64 <sub>0.63</sub> | 93.11 <sub>0.78</sub> | 93.11 <sub>0.78</sub> |
|                 |                     | IoU          | 83.78 <sub>1.39</sub> | 85.99 <sub>0.82</sub> | 85.50 <sub>0.54</sub>  | 87.54 <sub>1.21</sub> | 86.41 <sub>1.79</sub> | 86.35 <sub>1.19</sub> | 87.42 <sub>1.87</sub> | 86.34 <sub>1.51</sub> | 87.31 <sub>1.17</sub> | 86.33 <sub>1.90</sub> | 86.76 <sub>1.18</sub> | 86.61 <sub>1.16</sub> | 88.26 <sub>1.04</sub> | 87.44 <sub>1.17</sub> | 87.44 <sub>1.17</sub> |
|                 | S-UN                | DSC          | 91.54 <sub>0.58</sub> | 92.60 <sub>0.87</sub> | 92.69 <sub>0.70</sub>  | 93.84 <sub>0.17</sub> | 92.71 <sub>0.53</sub> | 93.30 <sub>0.35</sub> | 93.69 <sub>0.18</sub> | 92.94 <sub>0.45</sub> | 93.64 <sub>0.32</sub> | 93.07 <sub>0.65</sub> | 93.71 <sub>0.17</sub> | 93.30 <sub>0.54</sub> | 93.72 <sub>0.19</sub> | 93.77 <sub>0.16</sub> | 93.77 <sub>0.16</sub> |
|                 |                     | IoU          | 84.62 <sub>0.56</sub> | 86.70 <sub>1.36</sub> | 86.60 <sub>1.15</sub>  | 88.55 <sub>0.41</sub> | 86.59 <sub>0.89</sub> | 87.80 <sub>0.69</sub> | 88.27 <sub>0.88</sub> | 86.90 <sub>0.78</sub> | 88.22 <sub>0.89</sub> | 87.31 <sub>1.07</sub> | 88.31 <sub>0.81</sub> | 87.70 <sub>0.91</sub> | 88.35 <sub>0.84</sub> | 88.41 <sub>0.79</sub> | 88.41 <sub>0.79</sub> |
| DMF             | UN-P                | DSC          | 90.00 <sub>0.32</sub> | 90.10 <sub>0.31</sub> | 90.30 <sub>0.50</sub>  | 91.34 <sub>0.24</sub> | 90.53 <sub>0.50</sub> | 90.61 <sub>0.17</sub> | 91.24 <sub>0.41</sub> | 90.91 <sub>0.17</sub> | 91.35 <sub>0.19</sub> | 91.04 <sub>0.40</sub> | 91.01 <sub>0.15</sub> | 90.44 <sub>0.19</sub> | 91.22 <sub>0.49</sub> | 91.34 <sub>0.13</sub> |                       |
|                 |                     | IoU          | 82.87 <sub>0.79</sub> | 82.89 <sub>0.78</sub> | 83.31 <sub>0.74</sub>  | 84.76 <sub>0.67</sub> | 83.56 <sub>0.74</sub> | 83.62 <sub>0.71</sub> | 84.58 <sub>0.67</sub> | 84.10 <sub>0.69</sub> | 84.75 <sub>0.65</sub> | 84.29 <sub>0.68</sub> | 84.24 <sub>0.68</sub> | 83.30 <sub>0.71</sub> | 84.54 <sub>0.66</sub> | 84.74 <sub>0.66</sub> |                       |
|                 | A-UN                | DSC          | 90.06 <sub>0.17</sub> | 90.35 <sub>0.16</sub> | 90.54 <sub>0.15</sub>  | 91.31 <sub>0.13</sub> | 90.60 <sub>0.14</sub> | 90.67 <sub>0.16</sub> | 91.27 <sub>0.12</sub> | 90.53 <sub>0.50</sub> | 91.21 <sub>0.13</sub> | 90.38 <sub>0.18</sub> | 91.46 <sub>0.18</sub> | 90.56 <sub>0.16</sub> | 91.25 <sub>0.13</sub> | 91.37 <sub>0.14</sub> | 91.37 <sub>0.14</sub> |
|                 |                     | IoU          | 82.68 <sub>0.68</sub> | 83.15 <sub>0.69</sub> | 83.44 <sub>0.68</sub>  | 84.65 <sub>0.45</sub> | 83.68 <sub>0.68</sub> | 83.69 <sub>0.70</sub> | 84.59 <sub>0.64</sub> | 83.57 <sub>0.74</sub> | 84.50 <sub>0.66</sub> | 83.26 <sub>0.71</sub> | 84.92 <sub>0.65</sub> | 83.49 <sub>0.69</sub> | 84.58 <sub>0.66</sub> | 84.81 <sub>0.67</sub> | 84.81 <sub>0.67</sub> |
|                 | S-UN                | DSC          | 90.47 <sub>0.15</sub> | 91.17 <sub>0.15</sub> | 91.21 <sub>0.14</sub>  | 91.94 <sub>0.11</sub> | 91.24 <sub>0.15</sub> | 91.17 <sub>0.15</sub> | 91.67 <sub>0.11</sub> | 91.21 <sub>0.15</sub> | 91.84 <sub>0.11</sub> | 91.22 <sub>0.15</sub> | 91.67 <sub>0.14</sub> | 91.60 <sub>0.10</sub> | 92.08 <sub>0.10</sub> | 91.89 <sub>0.10</sub> | 91.89 <sub>0.10</sub> |
|                 |                     | IoU          | 83.30 <sub>0.67</sub> | 84.50 <sub>0.68</sub> | 84.49 <sub>0.65</sub>  | 85.72 <sub>0.51</sub> | 84.57 <sub>0.65</sub> | 84.43 <sub>0.65</sub> | 85.28 <sub>0.61</sub> | 84.56 <sub>0.68</sub> | 85.54 <sub>0.61</sub> | 84.59 <sub>0.68</sub> | 85.27 <sub>0.65</sub> | 85.23 <sub>0.62</sub> | 85.92 <sub>0.68</sub> | 85.92 <sub>0.68</sub> | 85.92 <sub>0.68</sub> |
| COL             | UN-P                | DSC          | 89.17 <sub>1.82</sub> | 89.59 <sub>1.81</sub> | 88.89 <sub>1.49</sub>  | 91.73 <sub>1.19</sub> | 90.56 <sub>1.86</sub> | 90.10 <sub>1.85</sub> | 91.64 <sub>1.21</sub> | 90.72 <sub>1.45</sub> | 91.03 <sub>1.19</sub> | 89.57 <sub>1.83</sub> | 90.73 <sub>1.11</sub> | 89.60 <sub>1.71</sub> | 90.62 <sub>1.63</sub> | 92.01 <sub>1.02</sub> |                       |
|                 |                     | IoU          | 82.93 <sub>0.85</sub> | 83.53 <sub>0.95</sub> | 81.99 <sub>1.06</sub>  | 86.01 <sub>1.36</sub> | 85.23 <sub>1.97</sub> | 84.40 <sub>1.84</sub> | 85.93 <sub>1.69</sub> | 84.81 <sub>1.81</sub> | 85.46 <sub>1.78</sub> | 83.69 <sub>0.98</sub> | 84.79 <sub>0.82</sub> | 83.45 <sub>0.99</sub> | 85.04 <sub>1.00</sub> | 86.24 <sub>1.45</sub> | 86.24 <sub>1.45</sub> |
|                 | A-UN                | DSC          | 89.25 <sub>1.94</sub> | 88.88 <sub>1.91</sub> | 89.19 <sub>1.86</sub>  | 91.37 <sub>1.17</sub> | 91.40 <sub>1.91</sub> | 89.76 <sub>1.89</sub> | 91.42 <sub>1.60</sub> | 90.10 <sub>1.90</sub> | 90.96 <sub>1.72</sub> | 89.00 <sub>0.88</sub> | 90.57 <sub>1.71</sub> | 89.84 <sub>1.79</sub> | 90.29 <sub>1.65</sub> | 91.20 <sub>1.50</sub> | 91.20 <sub>1.50</sub> |
|                 |                     | IoU          | 83.28 <sub>0.86</sub> | 81.91 <sub>1.15</sub> | 83.03 <sub>0.92</sub>  | 85.80 <sub>1.39</sub> | 85.15 <sub>1.43</sub> | 82.90 <sub>1.71</sub> | 86.19 <sub>1.88</sub> | 84.79 <sub>0.88</sub> | 85.64 <sub>1.88</sub> | 83.74 <sub>0.82</sub> | 85.06 <sub>1.91</sub> | 83.84 <sub>1.07</sub> | 84.51 <sub>1.39</sub> | 85.57 <sub>1.78</sub> | 85.57 <sub>1.78</sub> |
|                 | S-UN                | DSC          | 90.44 <sub>1.07</sub> | 91.02 <sub>1.10</sub> | 91.44 <sub>1.17</sub>  | 92.63 <sub>0.86</sub> | 91.90 <sub>1.19</sub> | 91.81 <sub>1.15</sub> | 92.70 <sub>0.87</sub> | 91.77 <sub>0.91</sub> | 91.72 <sub>1.10</sub> | 90.63 <sub>1.30</sub> | 92.10 <sub>1.17</sub> | 91.52 <sub>1.14</sub> | 92.55 <sub>1.00</sub> | 92.71 <sub>0.74</sub> | 92.71 <sub>0.74</sub> |
|                 |                     | IoU          | 83.64 <sub>1.49</sub> | 85.17 <sub>1.08</sub> | 85.68 <sub>1.36</sub>  | 86.96 <sub>1.08</sub> | 86.14 <sub>1.45</sub> | 86.01 <sub>1.45</sub> | 87.16 <sub>1.31</sub> | 86.54 <sub>1.34</sub> | 85.81 <sub>1.46</sub> | 84.35 <sub>0.63</sub> | 86.76 <sub>1.18</sub> | 86.00 <sub>1.07</sub> | 87.18 <sub>1.14</sub> | 87.01 <sub>1.15</sub> | 87.01 <sub>1.15</sub> |
| CLI             | UN-P                | DSC          | 92.01 <sub>1.18</sub> | 92.62 <sub>0.93</sub> | 92.67 <sub>1.00</sub>  | 93.80 <sub>0.83</sub> | 93.34 <sub>0.91</sub> | 92.98 <sub>0.71</sub> | 93.81 <sub>0.69</sub> | 92.53 <sub>0.96</sub> | 93.48 <sub>0.76</sub> | 92.27 <sub>1.03</sub> | 93.33 <sub>0.68</sub> | 92.55 <sub>0.81</sub> | 93.72 <sub>0.78</sub> | 93.64 <sub>0.77</sub> |                       |
|                 |                     | IoU          | 86.80 <sub>1.88</sub> | 87.70 <sub>1.85</sub> | 87.78 <sub>1.87</sub>  | 89.97 <sub>0.89</sub> | 88.61 <sub>1.09</sub> | 87.69 <sub>1.00</sub> | 89.09 <sub>0.83</sub> | 87.30 <sub>1.13</sub> | 88.64 <sub>0.81</sub> | 87.23 <sub>1.02</sub> | 88.21 <sub>0.84</sub> | 87.15 <sub>1.11</sub> | 89.00 <sub>0.98</sub> | 88.85 <sub>0.98</sub> |                       |
|                 | A-UN                | DSC          | 92.42 <sub>1.08</sub> | 92.96 <sub>1.08</sub> | 92.74 <sub>0.79</sub>  | 93.61 <sub>0.70</sub> | 93.04 <sub>1.01</sub> | 93.12 <sub>0.88</sub> | 93.98 <sub>0.68</sub> | 93.00 <sub>1.01</sub> | 93.67 <sub>0.79</sub> | 92.42 <sub>1.08</sub> | 93.57 <sub>0.71</sub> | 92.56 <sub>0.88</sub> | 93.36 <sub>0.70</sub> | 94.01 <sub>0.87</sub> | 94.01 <sub>0.87</sub> |
|                 |                     | IoU          | 87.38 <sub>1.21</sub> | 87.70 <sub>1.28</sub> | 88.15 <sub>0.99</sub>  | 88.76 <sub>0.86</sub> | 88.34 <sub>1.19</sub> | 88.16 <sub>1.08</sub> | 89.39 <sub>0.83</sub> | 88.26 <sub>1.19</sub> | 88.87 <sub>0.84</sub> | 87.31 <sub>1.22</sub> | 88.70 <sub>0.86</sub> | 87.29 <sub>1.15</sub> | 88.41 <sub>0.87</sub> | 89.23 <sub>0.82</sub> | 89.23 <sub>0.82</sub> |
|                 | S-UN                | DSC          | 91.08 <sub>1.08</sub> | 92.09 <sub>0.94</sub> | 92.34 <sub>0.95</sub>  | 93.38 <sub>0.80</sub> | 92.59 <sub>1.00</sub> | 92.84 <sub>0.94</sub> | 93.49 <sub>0.85</sub> | 93.00 <sub>0.95</sub> | 93.47 <sub>0.83</sub> | 92.70 <sub>0.93</sub> | 93.03 <sub>0.92</sub> | 91.51 <sub>1.07</sub> | 93.20 <sub>0.88</sub> | 93.36 <sub>0.88</sub> | 93.36 <sub>0.88</sub> |
|                 |                     | IoU          | 85.17 <sub>1.23</sub> | 86.60 <sub>1.19</sub> | 87.09 <sub>1.22</sub>  | 88.53 <sub>1.25</sub> | 87.61 <sub>1.24</sub> | 87.90 <sub>1.19</sub> | 88.83 <sub>1.09</sub> | 88.20 <sub>1.19</sub> | 88.75 <sub>1.07</sub> | 87.70 <sub>1.13</sub> | 88.17 <sub>1.15</sub> | 85.90 <sub>1.30</sub> | 88.41 <sub>1.14</sub> | 88.58 <sub>1.09</sub> | 88.58 <sub>1.09</sub> |

annealing with warm restarts (initial period 10 epochs, doubles after each restart) and early stopping (validation loss; patience 25 epochs) to minimize SmoothL1 loss (Eqn. 3) [13]. We set  $p_{\text{weak}} = 0.05$  (Sec. 2.2) and generate  $K = 50$  degraded masks per sample (Eqn. 1). On test sets,  $g_\phi$  achieves MAE in [0.043, 0.088] and Pearson’s correlation coefficient  $\rho > 0.92$  across all 5 datasets (Table 2  $\mathcal{A}$ ). Zeroing the image input in Eqn. 2, i.e.,  $g_\phi(x = \mathbf{0}, \tilde{y})$ , increases MAE by an average of  $0.399 \pm 0.137$  across all 5 datasets (MAE  $\in [0, 1]$ ), strongly confirming that  $g_\phi$  leverages image content (contextual grounding), rather than relying on the mask alone.

**SSL segmentation training and evaluation:** Next, we leverage our trained quality predictor to improve segmentation using semi-supervised learning (SSL). We evaluate 3 architectures for  $f_\theta$ : a purely convolutional model, U-Net++ [44] (UN-P; 26.08M parameters, 14.14 GFLOPs), a convolutional model with attention gates, Attention U-Net [26] (A-UN; 24.71M params, 6.16 GFLOPs), and a pure Transformer-based architecture, Swin-U-net [6] (S-UN; 34.27M params, 7.55 GFLOPs), optimizing Dice + cross-entropy loss (Eqn. 4) [16,37] for 200 epochs with AdamW (lr and weight decay set to 1e-4), a cosine annealing scheduler, and early stopping (validation DSC; patience of 30 epochs). We set  $\lambda_{\text{qar}} = 0.01$  and  $\lambda_{\text{qw}} = 0.25$  (Eqn. 6,8) and follow a ramp-up schedule during initial training epochs [39], and report Dice (DSC) and Jaccard (IoU) averaged

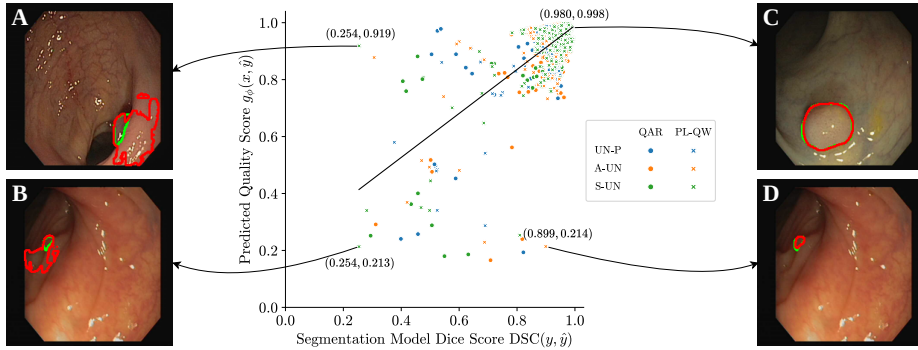


**Fig. 2.** Scatter plot of the segmentation predictions’ Dice  $DSC(y, \hat{y})$  and the corresponding predicted quality estimates  $g_\phi(x, \hat{y})$  on the test set of CLI dataset, and four representative images (A-D) with the ground truth (green) and predicted (red) segmentations. We observe a strong, stat. sig., positive linear correlation ( $\rho=0.69$ ;  $p=1e-314$ ).

over 3 runs with different seeds. We compare QAR (Sec. 2.4 A) against existing popular and widely used SSL paradigms: pseudolabels [19] with pixel-level confidence thresholded at 0.9 (PL-T), sample-level confidence-weighted pseudolabels [35] (PL-C), mean teacher [39] (MT) and its uncertainty-aware extension [42] (UA-MT), interpolation consistency training [41] (ICT), pseudolabel-based contrastive learning [7] (CL), and cross-pseudo supervision [9] (CPS). We do not compare against Zheng et al. [43], despite them incorporating quality estimation into SSL, because their code is not available. Nevertheless, we note that their estimator is trained end-to-end with the segmentation model and coupled to a specific self-training pipeline, whereas ours is the first framework-agnostic approach: an independently trained quality predictor that enhances any pseudolabel-generating method without architectural changes or retraining. Table 1 shows that QAR outperforms all competing SSL paradigms across all datasets and models, indicating that segmentation quality, even when predicted, may still be a better training signal than model confidence or uncertainty. It is important to note that the last two competing methods, CL and especially CPS (as it trains two segmentation models in tandem), are computationally more demanding. Despite no architectural modifications, QAR matches or surpasses state-of-the-art results on these datasets [11,36,12,21,27,20], many of which employ architectural innovations orthogonal to ours, suggesting further gains from combination.

**Quality weighting as a drop-in module:** Next, we show how our quality-weighted pseudolabels can be integrated with any approach that generates pseudolabels  $\hat{y}_j^u$  by weighting per-sample losses with  $w_j$  (Sec. 2.4 B). Concretely, for MT [39]:  $\mathcal{L}_{MT-QW} = \frac{1}{M} \sum_j w_j \|f_\theta(x_j^u) - \hat{y}_j^u\|^2$ ; for CPS [9]:  $\mathcal{L}_{CPS-QW} = \frac{1}{M} \sum_j [w_{j,2} \ell_{\text{seg}}(f_{\theta_1}(x_j^u), \hat{y}_{j,2}^u) + w_{j,1} \ell_{\text{seg}}(f_{\theta_2}(x_j^u), \hat{y}_{j,1}^u)]$ ; for ICT [41]:  $\mathcal{L}_{ICT-QW} = \frac{1}{M} \sum_j w_j \ell_{\text{seg}}(f_\theta(\tilde{x}_j^u), \tilde{y}_j^u)$ ; and for CL [7]:  $\mathcal{L}_{CPL-QW} = \frac{1}{M} \sum_j w_j [\ell_{\text{seg}}(f_\theta(x_j^u), \hat{y}_j^u) +$

**Table 2.** Ablation and hyperparameter sensitivity experiments. The values used for the main experiments table (Table 1) are highlighted. Results reported as mean<sub>std.err.</sub>. Unless specified otherwise,  $\mathcal{D}_L$  is PH2,  $\mathcal{D}_U$  is ISIC2020-Train,  $g_\phi$  is ResNet-18,  $f_\theta$  is Swin-Unet,  $p_{\text{weak}} = 0.05$ ,  $K = 50$ ,  $\lambda_{\text{qar}} = 0.01$ ,  $\lambda_{\text{qw}} = 0.25$ , and  $M = 5,000$ .  $e_{\text{val96}}$  denotes the number of training epochs for the validation DSC to reach 96%.

| A. $g_\phi$ 's metrics for all datasets  |                                |                                |                                |                                |                                |
|--|--------------------------------|--------------------------------|--------------------------------|--------------------------------|--------------------------------|
| Dataset  | PH2                            | SCD                            | DMF                            | COL                            | CLI                            |
| MAE / $\rho$   | 0.043 <sub>0.007</sub> / 0.972 | 0.052 <sub>0.007</sub> / 0.973 | 0.060 <sub>0.004</sub> / 0.926 | 0.074 <sub>0.007</sub> / 0.955 | 0.088 <sub>0.013</sub> / 0.927 |
| B. Varying $g_\phi$ 's backbones (Sec. 2.3)  |                                |                                |                                |                                |                                |
| Backbone   | MobileNetV3L                   | EfficientNet-B0                | ResNet-18                      | DenseNet-121                   | ConvNeXt-T                     |
| Params / FLOPs   | 4.53M / 0.24G                  | 4.34M / 0.42G                  | 11.31M / 1.87G                 | 7.22M / 2.95G                  | 28.02M / 4.47G                 |
| MAE / $\rho$   | 0.088 <sub>0.012</sub> / 0.849 | 0.054 <sub>0.009</sub> / 0.961 | 0.043 <sub>0.007</sub> / 0.972 | 0.089 <sub>0.011</sub> / 0.837 | 0.055 <sub>0.008</sub> / 0.955 |
| C. Varying $p_{\text{weak}}$ (i.e., probability of sampling from weak models' predictions; Sec. 2.2) |                                |                                |                                |                                |                                |
| $p_{\text{weak}}$  | 0.00                           | 0.05                           | 0.10                           | 0.15                           | 0.20                           |
| MAE / $\rho$   | 0.053 <sub>0.008</sub> / 0.960 | 0.043 <sub>0.007</sub> / 0.972 | 0.048 <sub>0.007</sub> / 0.965 | 0.049 <sub>0.007</sub> / 0.953 | 0.051 <sub>0.009</sub> / 0.948 |
| D. Varying $K$ (i.e., num. augmented training samples; Eqn. 1)                                       |                                |                                |                                |                                |                                |
| $K$  | 10                             | 20                             | 50                             | 100                            | 200                            |
| MAE / $\rho$   | 0.061 <sub>0.009</sub> / 0.937 | 0.048 <sub>0.006</sub> / 0.956 | 0.043 <sub>0.007</sub> / 0.972 | 0.047 <sub>0.006</sub> / 0.969 | 0.050 <sub>0.005</sub> / 0.977 |
| E. Impact of $p_{\text{weak}} > 0$ on segmentation performance                                       |                                |                                |                                |                                |                                |
| $p_{\text{weak}}$  | 0.00                           | 0.05                           | $p_{\text{weak}}$              | 0.00                           | 0.05                           |
| QAR: DSC   | 94.91 <sub>0.49</sub>          | 95.58 <sub>0.42</sub>          | PL-QW: DSC                     | 95.10 <sub>0.46</sub>          | 95.57 <sub>0.41</sub>          |
| F. Varying $\lambda_{\text{qar}}$ , i.e., relative weight of $\mathcal{L}_{\text{qar}}$ (Eqn. 6)     |                                |                                |                                |                                |                                |
| $\lambda_{\text{qar}}$   | 0.00                           | 0.01                           | 0.05                           | 0.10                           | 0.20                           |
| DSC  | 93.02 <sub>0.55</sub>          | 95.58 <sub>0.42</sub>          | 95.52 <sub>0.42</sub>          | 95.14 <sub>0.48</sub>          | 95.03 <sub>0.49</sub>          |
| G. Varying $\lambda_{\text{qw}}$ , i.e., relative weight of $\mathcal{L}_{\text{qw}}$ (Eqn. 8)       |                                |                                |                                |                                |                                |
| $\lambda_{\text{qw}}$  | 0.00                           | 0.25                           | 0.50                           | 0.75                           | 1.00                           |
| DSC  | 93.02 <sub>0.55</sub>          | 95.57 <sub>0.41</sub>          | 95.25 <sub>0.44</sub>          | 95.31 <sub>0.43</sub>          | 95.14 <sub>0.44</sub>          |
| H. Varying $M$ , i.e., number of unlabeled samples (Eqns. 5-8)                                       |                                |                                |                                |                                |                                |
| $M$  | 1,000                          | 5,000                          | 10,000                         | 20,000                         | 30,000                         |
| QAR: DSC / $e_{\text{val96}}$  | 95.48 <sub>0.43</sub> / 13     | 95.58 <sub>0.42</sub> / 2      | 95.36 <sub>0.43</sub> / 1      | 95.50 <sub>0.43</sub> / 1      | 95.36 <sub>0.45</sub> / 1      |
| PL-QW: DSC / $e_{\text{val96}}$  | 95.48 <sub>0.43</sub> / 12     | 95.57 <sub>0.41</sub> / 2      | 95.35 <sub>0.43</sub> / 2      | 95.48 <sub>0.43</sub> / 1      | 95.35 <sub>0.44</sub> / 1      |

$\lambda_c \mathcal{L}_{\text{contrast}}(x_j^u, \hat{y}_j^u)]$ , where quality weights both the pseudolabel loss and the contrastive loss. In all cases,  $w_j = g_\phi(x_j^u, \hat{y}_j^u)$  (with  $w_{j,k}$  evaluating the pseudolabel from network  $k$  in CPS). Table 1 shows that quality-weighted variants (\*-QW) consistently outperform original versions across all but one setting (DMF + UN-P), confirming the general applicability of our quality-weighting. A scatter plot of the calculated DSC and the predicted quality (Fig. 2), on CLI's test set across all 3 runs of both QAR and PL-QW, shows that the two are strongly correlated. Example images (A-D) show two successful  $g_\phi$  predictions for near-perfect (B) and poor (C) segmentations, and two failure cases for  $g_\phi$  (A, D).

**Ablation studies** (Table 2): Among 5 backbones from different architecture families, ResNet-18 performs the best for  $g_\phi$  (B). Incorporating weak-model corruptions (i.e.,  $p_{\text{weak}} > 0$ ) improves  $g_\phi$ 's performance (C), and increasing corrupted masks per sample (i.e.,  $K$ ) helps up to a saturation point (D).  $g_\phi$  trained with weak-model corruptions helps improve segmentation model performance for both QAR and PL-QW (E). Varying  $\lambda_{\text{qar}}$  and  $\lambda_{\text{qw}}$  (F, G) shows that even subop-

timal weights outperform the zero-weight baseline. Finally, increasing unlabeled data ( $\mathcal{H}$ ) has minimal impact on final DSC, but substantially accelerates convergence:  $e_{\text{val}96}$  (i.e., the number of epochs to reach 96% validation DSC) decreases considerably with larger  $M$ .

## 4 Conclusion

We presented a contextually-grounded deep learning-based approach to estimating the quality of medical image segmentations. Our quality predictor is trained on corrupted masks generated using synthetic degradations and weak segmentation models' predictions. We then integrated our quality predictor into existing semi-supervised learning (SSL)-based segmentation frameworks through two complementary mechanisms: either as a regularization loss or as a sample reweighting mechanism, without any architectural modifications to the segmentation network. Extensive experiments across multiple datasets and model architectures demonstrated consistent improvements over existing SSL paradigms, confirming that learned quality prediction provides an effective training signal for leveraging unlabeled data. Future work could explore extending quality-guided SSL to multi-class segmentation, and leveraging quality predictions for active learning to identify unlabeled samples to be prioritized for expert annotation.

**Acknowledgments.** The authors thank Darren Sutton for initial discussions and acknowledge computational support from NVIDIA Corporation and the Digital Research Alliance of Canada. Partial funding for this project was provided by the Natural Sciences and Engineering Research Council of Canada (NSERC RGPIN-2020-06752).

**Disclosure of Interests.** The authors have no competing interests to declare.

## References

1. Asgari Taghanaki, S., Abhishek, K., Cohen, J.P., Cohen-Adad, J., Hamarneh, G.: Deep semantic segmentation of natural and medical images: a review. *Artificial intelligence review* **54**(1), 137–178 (Jun 2021). <https://doi.org/10.1007/s10462-020-09854-1>
2. Ballerini, L., Fisher, R.B., Aldridge, B., Rees, J.: A Color and Texture Based Hierarchical K-NN Approach to the Classification of Non-melanoma Skin Lesions. In: Celebi, M.E., Schaefer, G. (eds.) *Color Medical Image Analysis*. vol. 6, pp. 63–86. Springer Netherlands (2013). [https://doi.org/10.1007/978-94-007-5389-1\\_4](https://doi.org/10.1007/978-94-007-5389-1_4)
3. Bernal, J., Sánchez, F.J., Fernández-Esparrach, G., Gil, D., Rodríguez, C., Vilarino, F.: Wm-dova maps for accurate polyp highlighting in colonoscopy: Validation vs. saliency maps from physicians. *Computerized Medical Imaging and Graphics* **43**, 99–111 (Jul 2015). <https://doi.org/10.1016/j.compmedimag.2015.02.007>
4. Bernal, J., Sánchez, J., Vilarino, F.: Towards automatic polyp detection with a polyp appearance model. *Pattern Recognition* **45**(9), 3166–3182 (Sep 2012). <https://doi.org/10.1016/j.patcog.2012.03.002>

5. Byrne, N., Clough, J.R., Montana, G., King, A.P.: A persistent homology-based topological loss function for multi-class CNN segmentation of cardiac MRI. In: *Statistical Atlases and Computational Models of the Heart. M&Ms and EMIDEC Challenges*. p. 3–13. Springer International Publishing (2021). [https://doi.org/10.1007/978-3-030-68107-4\\_1](https://doi.org/10.1007/978-3-030-68107-4_1)
6. Cao, H., Wang, Y., Chen, J., Jiang, D., Zhang, X., Tian, Q., Wang, M.: Swin-Unet: Unet-like pure transformer for medical image segmentation. In: *European Conference on Computer Vision*. pp. 205–218. Springer (2022). [https://doi.org/10.1007/978-3-031-25066-8\\_9](https://doi.org/10.1007/978-3-031-25066-8_9)
7. Chaitanya, K., Erdil, E., Karani, N., Konukoglu, E.: Local contrastive loss with pseudo-label based self-training for semi-supervised medical image segmentation. *Medical Image Analysis* **87**, 102792 (Jul 2023). <https://doi.org/10.1016/j.media.2023.102792>
8. Chen, S., Urban, G., Baldi, P.: Weakly supervised polyp segmentation in colonoscopy images using deep neural networks. *Journal of Imaging* **8**(5), 121 (Apr 2022). <https://doi.org/10.3390/jimaging8050121>
9. Chen, X., Yuan, Y., Zeng, G., Wang, J.: Semi-Supervised Semantic Segmentation with Cross Pseudo Supervision. In: *2021 IEEE/CVF Conference on Computer Vision and Pattern Recognition (CVPR)*. pp. 2613–2622. IEEE, Nashville, TN, USA (Jun 2021). <https://doi.org/10.1109/CVPR46437.2021.00264>
10. DeVries, T., Taylor, G.W.: Leveraging uncertainty estimates for predicting segmentation quality. *arXiv preprint arXiv:1807.00502* pp. 1–9 (Jul 2018)
11. Du, S., Bayasi, N., Hamarneh, G., Garbi, R.: MDViT: Multi-domain vision transformer for small medical image segmentation datasets. In: *Medical Image Computing and Computer Assisted Intervention – MICCAI 2023*. p. 448–458. Springer Nature Switzerland (2023). [https://doi.org/10.1007/978-3-031-43901-8\\_43](https://doi.org/10.1007/978-3-031-43901-8_43)
12. Dzieniszewska, A., Garbat, P., Piramidowicz, R.: Improving skin lesion segmentation with self-training. *Cancers* **16**(6), 1120 (Mar 2024). <https://doi.org/10.3390/cancers16061120>
13. Girshick, R.: Fast R-CNN. In: *2015 IEEE International Conference on Computer Vision (ICCV)*. p. 1440–1448. IEEE (Dec 2015). <https://doi.org/10.1109/iccv.2015.169>
14. Glaister, J., Amelard, R., Wong, A., Clausi, D.A.: MSIM: Multistage illumination modeling of dermatological photographs for illumination-corrected skin lesion analysis. *IEEE Transactions on Biomedical Engineering* **60**(7), 1873–1883 (Jul 2013). <https://doi.org/10.1109/tbme.2013.2244596>
15. Guo, C., Pleiss, G., Sun, Y., Weinberger, K.Q.: On calibration of modern neural networks. In: *International Conference on Machine Learning*. pp. 1321–1330. PMLR (2017)
16. Isensee, F., Jaeger, P.F., Kohl, S.A., Petersen, J., Maier-Hein, K.H.: nnU-Net: a self-configuring method for deep learning-based biomedical image segmentation. *Nature Methods* **18**(2), 203–211 (Feb 2021). <https://doi.org/10.1038/s41592-020-01008-z>
17. Kirillov, A., Wu, Y., He, K., Girshick, R.: PointRend: Image segmentation as rendering. In: *2020 IEEE/CVF Conference on Computer Vision and Pattern Recognition (CVPR)*. p. 9796–9805. IEEE (Jun 2020). <https://doi.org/10.1109/cvpr42600.2020.00982>
18. Kohlberger, T., Singh, V., Alvino, C., Bahlmann, C., Grady, L.: Evaluating Segmentation Error without Ground Truth. In: *Hutchison, D., Kanade, T., Kittler, J., Kleinberg, J.M., Mattern, F., Mitchell, J.C., Naor, M., Nierstrasz, O.,*

- Pandu Rangan, C., Steffen, B., Sudan, M., Terzopoulos, D., Tygar, D., Vardi, M.Y., Weikum, G., Ayache, N., Delingette, H., Golland, P., Mori, K. (eds.) Medical Image Computing and Computer-Assisted Intervention – MICCAI 2012. vol. 7510, pp. 528–536. Springer Berlin Heidelberg, Berlin, Heidelberg (2012). [https://doi.org/10.1007/978-3-642-33415-3\\_65](https://doi.org/10.1007/978-3-642-33415-3_65)
19. Lee, D.H.: Pseudo-Label : The Simple and Efficient Semi-Supervised Learning Method for Deep Neural Networks. In: ICML 2013 Workshop on Challenges in Representation Learning. vol. 3 (2), pp. 1–6. Atlanta, Georgia, USA (Jun 2013)
  20. Li, Y., Tian, T., Hu, J., Yuan, C.: SUTrans-NET: a hybrid transformer approach to skin lesion segmentation. *PeerJ Computer Science* **10**, e1935 (Mar 2024). <https://doi.org/10.7717/peerj-cs.1935>
  21. Liang, P., Chen, J., Wu, Y., Wu, R., Chen, Z., Pu, B., Chang, Q., Ran, G.: A multilevel alignment and cross-fusion knowledge distillation framework for vision transformer-based medical image segmentation. *Future Generation Computer Systems* **177**, 108228 (Apr 2026). <https://doi.org/10.1016/j.future.2025.108228>
  22. Litjens, G., Kooi, T., Bejnordi, B.E., Setio, A.A.A., Ciompi, F., Ghafoorian, M., Van Der Laak, J.A., Van Ginneken, B., Sánchez, C.I.: A survey on deep learning in medical image analysis. *Medical Image Analysis* **42**, 60–88 (Dec 2017). <https://doi.org/10.1016/j.media.2017.07.005>
  23. Loshchilov, I., Hutter, F.: Decoupled weight decay regularization. In: International Conference on Learning Representations (2019), <https://openreview.net/forum?id=Bkg6RiCqY7>
  24. Mehrtash, A., Wells, W.M., Tempany, C.M., Abolmaesumi, P., Kapur, T.: Confidence calibration and predictive uncertainty estimation for deep medical image segmentation. *IEEE Transactions on Medical Imaging* **39**(12), 3868–3878 (Dec 2020). <https://doi.org/10.1109/tmi.2020.3006437>
  25. Mendonça, T., Ferreira, P.M., Marques, J.S., Marcal, A.R.S., Rozeira, J.: PH<sup>2</sup> - A dermoscopic image database for research and benchmarking. In: IEEE Engineering in Medicine and Biology Society. pp. 5437–5440 (Jul 2013). <https://doi.org/10.1109/embc.2013.6610779>
  26. Oktay, O., Schlemper, J., Folgoc, L.L., Lee, M., Heinrich, M., Misawa, K., Mori, K., McDonagh, S., Hammerla, N.Y., Kainz, B., Glocker, B., Rueckert, D.: Attention u-net: Learning where to look for the pancreas. In: Medical Imaging with Deep Learning (2018), <https://openreview.net/forum?id=Skft7cijM>
  27. Perera, S., Erzurumlu, Y., Gulati, D., Yilmaz, A.: MobileUNETR: A lightweight end-to-end hybrid vision transformer for efficient medical image segmentation. In: Computer Vision – ECCV 2024 Workshops. p. 281–299. Springer Nature Switzerland (2025). [https://doi.org/10.1007/978-3-031-91721-9\\_18](https://doi.org/10.1007/978-3-031-91721-9_18)
  28. Qiu, P., Chakrabarty, S., Nguyen, P., Ghosh, S.S., Sotiras, A.: QCResUNet: Joint Subject-Level and Voxel-Level Prediction of Segmentation Quality. In: Greenspan, H., Madabhushi, A., Mousavi, P., Salcudean, S., Duncan, J., Syeda-Mahmood, T., Taylor, R. (eds.) Medical Image Computing and Computer Assisted Intervention – MICCAI 2023. vol. 14223, pp. 173–182. Springer Nature Switzerland, Cham (2023). [https://doi.org/10.1007/978-3-031-43901-8\\_17](https://doi.org/10.1007/978-3-031-43901-8_17)
  29. Ren, M., Zeng, W., Yang, B., Urtasun, R.: Learning to reweight examples for robust deep learning. In: International Conference on Machine Learning. pp. 4334–4343. PMLR (2018)
  30. Robinson, R., Oktay, O., Bai, W., Valindria, V.V., Sanghvi, M.M., Aung, N., Paiva, J.M., Zemrak, F., Fung, K., Lukaschuk, E., et al.: Real-time prediction

- of segmentation quality. In: International Conference on Medical Image Computing and Computer-Assisted Intervention. pp. 578–585. Springer (2018). [https://doi.org/10.1007/978-3-030-00937-3\\_66](https://doi.org/10.1007/978-3-030-00937-3_66)
31. Ronneberger, O., Fischer, P., Brox, T.: U-net: Convolutional networks for biomedical image segmentation. In: International Conference on Medical image computing and computer-assisted intervention. pp. 234–241. Springer (2015). [https://doi.org/10.1007/978-3-319-24574-4\\_28](https://doi.org/10.1007/978-3-319-24574-4_28)
  32. Rotemberg, V., Kurtansky, N., Betz-Stablein, B., Caffery, L., Chousakos, E., Codella, N., Combalia, M., Dusza, S., Guitera, P., Gutman, D., Halpern, A., Helba, B., Kittler, H., Kose, K., Langer, S., Lioprys, K., Malvey, J., Musthaq, S., Nanda, J., Reiter, O., Shih, G., Stratigos, A., Tschandl, P., Weber, J., Soyer, H.P.: A patient-centric dataset of images and metadata for identifying melanomas using clinical context. *Scientific Data* **8**(1), 34 (Jan 2021). <https://doi.org/10.1038/s41597-021-00815-z>
  33. Senbi, A., Huang, T., Lyu, F., Li, Q., Tao, Y., Shao, W., Chen, Q., Wang, C., Wang, S., Zhou, T., Zhang, Y.: Towards ground-truth-free evaluation of any segmentation in medical images. arXiv preprint arXiv:2409.14874 pp. 1–17 (2024)
  34. Shu, J., Xie, Q., Yi, L., Zhao, Q., Zhou, S., Xu, Z., Meng, D.: Meta-weight-net: Learning an explicit mapping for sample weighting. *Advances in Neural Information Processing Systems* **32** (2019)
  35. Sohn, K., Berthelot, D., Carlini, N., Zhang, Z., Zhang, H., Raffel, C.A., Cubuk, E.D., Kurakin, A., Li, C.L.: FixMatch: Simplifying semi-supervised learning with consistency and confidence. *Advances in Neural Information Processing Systems* **33**, 596–608 (2020)
  36. Song, P., Wang, Z., Zhang, J., Fu, S., Zhang, Y., Wu, W., Bao, F.: SU-RMT: Toward bridging semantic representation and structural detail modeling for medical image segmentation. *Information Fusion* **131**, 104182 (Jul 2026). <https://doi.org/10.1016/j.inffus.2026.104182>
  37. Taghanaki, S.A., Zheng, Y., Zhou, S.K., Georgescu, B., Sharma, P., Xu, D., Comaniciu, D., Hamarneh, G.: Combo loss: Handling input and output imbalance in multi-organ segmentation. *Computerized Medical Imaging and Graphics* **75**, 24–33 (Jul 2019). <https://doi.org/10.1016/j.compmedimag.2019.04.005>
  38. Tajbakhsh, N., Jeyaseelan, L., Li, Q., Chiang, J.N., Wu, Z., Ding, X.: Embracing imperfect datasets: A review of deep learning solutions for medical image segmentation. *Medical image analysis* **63**, 101693 (Jul 2020). <https://doi.org/10.1016/j.media.2020.101693>
  39. Tarvainen, A., Valpola, H.: Mean teachers are better role models: Weight-averaged consistency targets improve semi-supervised deep learning results. In: Guyon, I., Luxburg, U.V., Bengio, S., Wallach, H., Fergus, R., Vishwanathan, S., Garnett, R. (eds.) *Advances in Neural Information Processing Systems*. vol. 30. Curran Associates, Inc. (2017)
  40. Valindria, V.V., Lavdas, I., Bai, W., Kamnitsas, K., Aboagye, E.O., Rockall, A.G., Rueckert, D., Glocker, B.: Reverse Classification Accuracy: Predicting Segmentation Performance in the Absence of Ground Truth. *IEEE Transactions on Medical Imaging* **36**(8), 1597–1606 (Aug 2017). <https://doi.org/10.1109/TMI.2017.2665165>
  41. Verma, V., Kawaguchi, K., Lamb, A., Kannala, J., Solin, A., Bengio, Y., Lopez-Paz, D.: Interpolation consistency training for semi-supervised learning. *Neural Networks* **145**, 90–106 (Jan 2022). <https://doi.org/10.1016/j.neunet.2021.10.008>

42. Yu, L., Wang, S., Li, X., Fu, C.W., Heng, P.A.: Uncertainty-Aware Self-ensembling Model for Semi-supervised 3D Left Atrium Segmentation. In: Shen, D., Liu, T., Peters, T.M., Staib, L.H., Essert, C., Zhou, S., Yap, P.T., Khan, A. (eds.) *Medical Image Computing and Computer Assisted Intervention – MICCAI 2019*. vol. 11765, pp. 605–613. Springer International Publishing, Cham (2019). [https://doi.org/10.1007/978-3-030-32245-8\\_67](https://doi.org/10.1007/978-3-030-32245-8_67)
43. Zheng, Z., Wang, X., Zhang, X., Zhong, Y., Yao, X., Zhang, Y., Wang, Y.: Semi-supervised segmentation with self-training based on quality estimation and refinement. In: *Machine Learning in Medical Imaging*. p. 30–39. Springer International Publishing (2020). [https://doi.org/10.1007/978-3-030-59861-7\\_4](https://doi.org/10.1007/978-3-030-59861-7_4), [http://dx.doi.org/10.1007/978-3-030-59861-7\\_4](http://dx.doi.org/10.1007/978-3-030-59861-7_4)
44. Zhou, Z., Siddiquee, M.M.R., Tajbakhsh, N., Liang, J.: Unet++: Redesigning skip connections to exploit multiscale features in image segmentation. *IEEE Transactions on Medical Imaging* **39**(6), 1856–1867 (2019). <https://doi.org/10.1109/tmi.2019.2959609>